Chemical Physics Letters 732 (2019) 136645

Contents lists available at ScienceDirect

Chemical Physics Letters

journal homepage: www.elsevier.com/locate/cplett

Research paper

Existence of dimeric hydroxylamine-O-sulfonic acid: Experimental observations aided by *ab initio*, DFT, Car-Parrinello and Born – Oppenheimer on the fly dynamics

Bipan Dutta[a], Joydeep Chowdhury[b,*]

[a] Department of Physics, Sammilani Mahavidyalaya, E.M. Bypass, Baghajatin Station, Kolkata 700094, India
[b] Department of Physics, Jadavpur University, Kolkata 700032, India

HIGHLIGHTS

- The Raman and temperature dependent FTIR spectra of HOSA molecule have been recorded.
- Complete vibrational analyses of the molecule have been estimated from *ab initio* and DFT calculations.
- The explicit presence of D2 form of the molecule has been reveal by IR spectra recorded at high temperatures.
- The dynamics of hydrogen bonded complex formation or destruction as been estimated from the CPMD calculations.

ARTICLE INFO

Keywords:
Hydroxylamine-O-sulfonic acid
FTIR
Raman
Ab Initio
CPMD
BOMD

ABSTRACT

This paper reports detail study on the Raman and temperature dependent IR spectra of hydroxylamine-O-sulfonic acid molecule. Complete vibrational analyses of the molecule have been reported based on *ab initio* calculations. Raman and IR spectra captured at room temperature suggest the presence of both the dimeric D1 and D2 forms of the molecule. However, the IR spectra of the molecule recorded at elevated temperatures mark the explicit presence of the D2 form of the molecule. The theoretically simulated temperature dependent dynamic IR spectra have the capability to predict the dynamics of hydrogen bonded complex formation or destruction under external perturbation.

1. Introduction

While covalent bonds and electrostatic interactions are the key forces that primarily hold the atoms in molecules, non-covalent interactions especially that prevail in hydrogen (H) bonds play significant roles in various biochemical processes [1–5]. These H-bond interactions also help in promoting the necessary thermodynamic stabilities towards the formation of supramolecular and macromolecular architectures [6,7]. For example, the intermolecular hydogen (IMH) bonds between the purine and pyrimidine bases not only embrace the DNA strands following Chargaff's rule, but also decide the orientations of the nucleotide bases amid pentose sugar and phosphate backbones. Moreover non-covalent IMH bonds also take part in the formation of molecular complexes [8,9]. The most successful and traditional ways to perceive IMH bonds in molecules have been the identification of the concerned vibrational signatures, as traced from their respective Raman and Fourier transform infrared (FTIR) spectra [10–14].

Nowadays *ab initio* molecular dynamics (AIMD) simulations play significant role to substantiate the available experimental results as obtained from Raman and FTIR spectra [15]. Born – Oppenheimer molecular dynamics (BOMD) and Car-Parrinello molecular dynamics (CPMD) are commonly applied *ab initio* molecular dynamics techniques that have been successfully used to understand the inherent dynamics involved in the H bonded molecular systems [16,17]. In BOMD calculations, the electronic energy of the molecular system is minimized and then the electronic properties of the system are estimated at each step. Within Born Oppenheimer (BO) approximation, the interaction energy in molecular dynamics calculations represents the Kohn Sham (KS) energy which in turn depends on the nuclear positions of the concerned molecular system. The potential energy hypersurface of the molecular system is thus generated from the movement of the nuclei [16].

In contrast to BOMD, the CPMD approach is based on the electronic optimization method, where a fictitious electronic mass is assigned to the propagating orbitals of the electrons. In this approach the

* Corresponding author.
E-mail address: joydeep72_c@rediffmail.com (J. Chowdhury).

https://doi.org/10.1016/j.cplett.2019.136645
Received 16 May 2019; Received in revised form 26 July 2019; Accepted 29 July 2019
Available online 30 July 2019
0009-2614/

information relating to the separation of time scales that remain ingrained between the quick motions of lighter electrons and the slower motions of the heavy nuclei are extracted. The inter nuclear distances act as parameter rather than variable for respective time scales in the simulation run at the expense of the explicit time-dependence relating the quantum subsystem dynamics [17].

Hydroxylamine-O-sulfonic acid (HOSA) is an important organic compound often used as a potential reagent in synthetic organic chemistry [18].The amine group ($-NH_2$) present in the HOSA molecule can act both as nucleophile and electrophile in chemical reactions. HOSA is successfully used in amination and reductive deamination reactions, in nitrile and in oxime formations, and in the preparation of amides and diazo compounds [18]. Interestingly, HOSA participates as reaction centre towards the synthesis of mono -, di – substituted hydrazines, trisubstituted hydrazinium salts and in nitrogen containing heterocycles like pyridine, quonoiline, pyrazine, etc. [18]. Considering enormous chemical applications of HOSA in organic chemistry, the present paper reports a detail study on the IR spectra of the molecule recorded both at room and at high temperatures. The Raman spectrum of the molecule in the solid state at room temperature is also reported herewith. Complete vibrational analyses of the HOSA molecule aided by *ab initio* quantum chemical calculations and simulation of dynamic IR spectra from CPMD and BOMD are reported for the first time in this paper. The preferential existences of the different dimeric forms of HOSA molecule at various temperature domains have also been estimated from the experimental observations with the aid of CPMD [19,20] and BOMD [16] simulation studies.

2. Instrumentation

The Raman spectrum of HOSA molecule has been recorded with a Renishaw Raman Microscope, equipped with a He-Ne laser excitation source emitting at a wavelength of 632.8 nm, and a Peltier cooled (−70 °C) charge coupled device (CCD) camera. A Leica microscope was attached and was fitted with three objectives (5×, 20×, and 50×). For these experiments, the 20× objective was used to focus the laser beam onto a spot of 1–2 μm^2. Laser power at the sample was 20 mW, and the data acquisition time was 30 s. The holographic grating (1800 grooves/mm) and the slit enabled the spectral resolution of 1 cm^{-1}. The mid-infrared spectra from 400 to 4000 cm^{-1} of the HOSA molecule in solid state was recorded on a Perkin-Elmer model Spectrum 100 fourier transform spectrometer equipped with a nichrome wire source, Ge/CsI beamsplitter and DTGS detector. Atmospheric water vapor was removed from the spectrometer chamber by purging with dry nitrogen. The interferograms were recorded at variable temperatures ranging from 40 °C to 145 °C with 4 scans and transformed by a Blackman-Harris apodization function with a theoretical resolution of 1.0 cm^{-1}. The temperature studies were carried out in a specially designed cryostat cell, which is composed of a copper cell with a 4 μm path length and wedged silicon windows sealed to the cell with indium gaskets. The temperature was monitored by two platinum thermal resistors and the cell was cooled by the vapors from boiling liquid nitrogen. The FTIR spectrum of the annealed sample was achieved by heating the cell in vacuum until the temperature was reached at 145 °C. When the desired temperature was achieved, the cell was allowed to cool down to room temperature and the spectrum was recorded.

3. Theoretical calculations

The theoretical calculations were carried out using Gaussion-09 suite of program [21]. The vibrational frequencies of the monomeric and dimeric forms of the HOSA molecule at their respective optimized geometries were computed by the second order Møller-Plesset (MP2) [22] levels of theory. Very tight criterion has been employed in the process of geometry optimization for fully relaxed method. All the calculations converge and the absence of imaginary frequencies in the calculated wavenumbers confirmed the attainment of local minima on the potential energy surface. The theoretically estimated vibrational frequencies, as obtained from the *ab initio* MP2/aug-cc-pVTZ level of theory, were scaled by the scaling factor of 0.994. The vibrational frequencies for the dimeric forms of the HOSA molecule are also estimated from anharmonic DFT calculations at B3LYP/aug-cc-pVTZ level of theory. The potential energy distributions (PEDs) associated with the normal modes of vibrations for the monomeric and dimeric forms of the HOSA molecule were estimated from the output of the *ab initio* and DFT calculations using GAR2PED software [23].

Ab initio molecular dynamics (MD) simulations have been carried out using CPMD programme [24] with the pre-optimized various monomer and dimeric molecular structures of the HOSA molecule. Each of the monomeric and dimeric structures of HOSA molecule is placed at the centre of a simple cubic cell of dimension 10.0 × 10.0 × 10.0 $Å^3$. The NVT ensemble has been chosen to execute the simulation at room temperature over an equilibrium time of 10 picoseconds. The time step was set to 4.0 a.u. that corresponds to ~0.096 fs. The Nose-Hoover thermostat [25,26] has been used to control the temperature of the NVT ensemble. However, an electronic fictitious mass of 500 a.u. has been used only for CPMD simulation. The gradient corrected Perdew, Burke and Ernzerhof (PBE) functional [27] has been utilized to model the electronic exchange and correlation factors. Core electrons were treated with pseudo potentials (PP) of Troullier and Martins [28], while valance electrons were represented by plane-wave basis set truncated at an energy cutoff of 80 Ry.

The dynamic IR or power spectra for the monomeric and dimeric forms of HOSA molecule at room and at high temperature domains have been estimated from the dipole moments, as obtained from the CPMD and BOMD trajectories. The dynamic IR spectra have been simulated from Fourier transform of the dipole moments of the auto-correlation function [DMAF].

The time average $C(t)$of DMAF is expressed as:

$$C(t) = \langle \mu(0)\mu(t) \rangle \tag{1}$$

where μ(0) and μ(t) are the dipole moments of the molecule estimated at initial and final times t respectively.

The dipole moment μ (t) is known to be strongly correlated with the dipole moment μ (0) within a short period of time [29]. The spectral density of the system is then calculated from the Fourier transform of the correlation function of the dipole moment.

The dynamic IR spectrum is represented as:

$$I(\omega) = \frac{h\beta}{(2\pi)^2}\omega^2 \int dt e^{-i\omega t}\langle \mu(0)\mu(t) \rangle \tag{2}$$

where I, ω, h, and β represent the IR Intensity, frequency, Planck constant and inverse of the Boltzmann constant respectively. The dipole moment (μ) of the molecule at successive time steps ~0.096 fs has been obtained from CPMD and BOMD simulation studies. To get the more accurate IR intensity, the quantum correlation factor (QCF) of the form $\frac{\beta h\omega}{(1-e^{-\beta h\omega})}$ has been used [30]. The evolution of N—H stretching band contours with time as extracted from the CPMD and BOMD trajectories of the dimeric form of HOSA molecule at various temperatures are estimated using TRAVIS software [31].

4. Results and discussion

4.1. Molecular structure

HOSA molecule is known to exist in two monomeric [ca. neutral (N) and zwitterion (Z)] and also in dimeric D1, D2 forms [32]. The

Table 1
Calculated Interaction energies (IEs) of the hydrogen bonded complexes of the HOSA molecule as obtained from *ab initio* MP2/aug-cc-PVTZ level of theory.

Combinations	ΔE_{int} (kcal/mol)
D1 – N – N	−1.88
D1 – ZW – ZW	−2.57
D2 – N – N	−1.88
D2 – ZW – ZW	−2.57
D1 – N – ZW	−2.25
D2 – N – ZW	−2.13

occurrence of D1, D2 dimers may be associated with N—N, Z—Z and/or N—Z forms of the molecule bridging through IMH bonds. The interaction energies (IE) of each of these hydrogen bonded complexes have been estimated from the following relation:

$$\Delta E_{int} = E_{D_i}^{D_i} - E_{M_i}^{D_i} - E_{M_j}^{D_i} \quad (3)$$

where $E_{D_i}^{D_i}$ represents the total SCF energy of the i^{th} dimeric complex. $E_{M_i}^{D_i}$ and $E_{M_j}^{D_i}$ signify the total SCF energies of the i^{th} and j^{th} monomeric forms of the molecule. All the SCF energies are calculated using aug-cc-pVTZ basis set at MP2 level of theory and are shown in Table 1. The basis set superposition error (BSSE) for the IEs has been corrected using counterpoise method. From Table 1, it is clearly seen that ΔE_{int} for both the dimeric D1 and D2 forms involving the Z - forms of the HOSA molecule show minimum SCF energies. These results may signify the dimeric D1, D2 forms associated with two Z-monomeric form of the HOSA molecule are considered to be stable. The optimized molecular structures and the relative changes in the MP2 energies (ΔE) of the monomeric N, Z and dimeric D1, D2 forms of the molecule are shown in Fig. 1. The estimated MP2 energy of the Z - form is ~6.2 kcal/mole higher than the corresponding N - form of the molecule. The two dimeric D1, D2 forms of the molecule are energetically separated by slender energy gap of 0.15 kcal/mole.

4.2. Raman, temperature dependent FTIR spectrum of the HOSA molecule and their vibrational assignment:

Fig. 2(a) shows the experimentally observed Raman spectrum of HOSA molecule in solid state recorded at room temperature. The theoretically simulated Raman spectra of D1, D2 dimeric and mixed forms of the molecule are shown in Fig. 2(b, c and d). Complete vibrational analyses of the Raman and IR bands (which will be discussed shortly) of HOSA molecule recorded at room temperature are presented in Table 2. The vibrational analyses of the monomeric N- and Z- forms of the molecule, as obtained from *ab initio* calculations, are also shown in Table S1. Raman spectrum of HOSA is marked by well resolved structured bands both in low as well as in the high wavenumber windows. The most prominent peaks in the low wavenumber region spanning from 100 to 1700 cm^{-1} are recorded at ~994 and 1053 cm^{-1}. The former band 994 cm^{-1} [calcd. at 1029/1016 cm^{-1} (MP2/aug-cc-pVTZ), 991 cm^{-1} (B3LYP/aug-cc-pVTZ) for D1 and 1029/1017 cm^{-1} (MP2/aug-cc-pVTZ), 1010/1011 cm^{-1} (B3LYP/aug-cc-pVTZ) for D2 form of the HOSA molecule] predominantly steers from ν(ON) and $\nu_s(SO_3)$ stretching vibrations associated with the D1 and D2 dimeric forms of the molecule. Interestingly D1 form of the molecule belongs to C_i point group symmetry [Refer to Fig. 1(c)], while its D2 form loses the point of inversion [Refer to Fig. 1(d)] and settles to C_2 point group. Nonetheless, intense Raman band at ~994 cm^{-1} represents totally symmetric vibrations originating from 'A_g' and 'A' irreducible representations of the D1 and D2 forms of the molecule respectively. The other Raman band at ~1053 cm^{-1} [calcd. at 1045/1046 cm^{-1} (MP2/aug-cc-pVTZ), for D1 and 1044/1046 cm^{-1} (MP2/aug-cc-pVTZ) for D2 form of the HOSA molecule] is owed to ν(ON), $\nu_s(SO_3)$ stretching and symmetric $\delta_{sym}(NH_3)$ deformation vibrations emanating either from

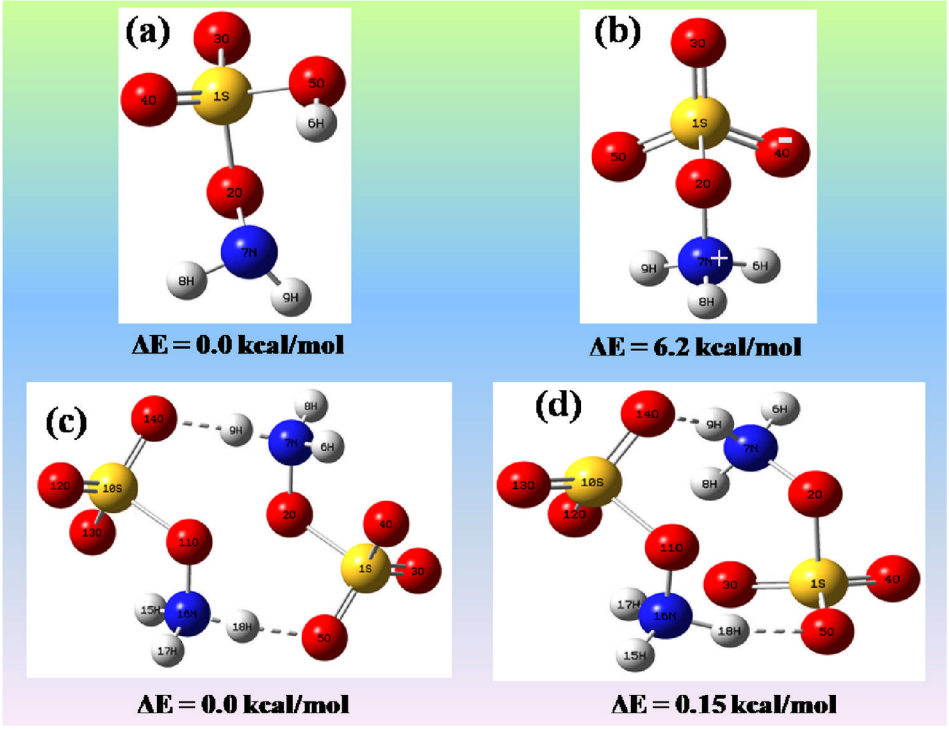

Fig. 1. Optimized molecular structures and respective SCF energy changes (ΔE) of (a) N-, (b) Z-monomeric and (c) D1, d) D2 dimeric forms of the HOSA molecule as obtained from *ab initio* MP2/aug-cc-PVTZ level of theory.

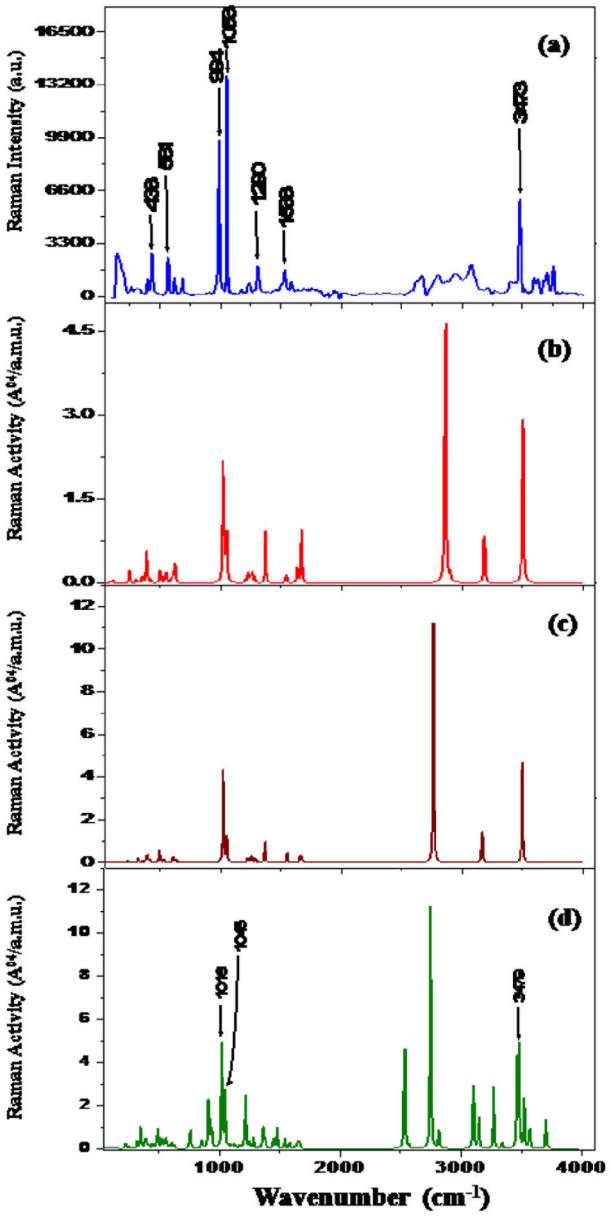

Fig. 2. (a) Raman spectrum of HOSA molecule in the solid state recorded at 100–4000 cm^{-1} region for λ_{exc} = 632.8 nm. Theoretically simulated gas- phase Raman spectra of (b) D1, (c) D2 and d) mixture of D1, D2 forms of the HOSA molecule using *ab initio* MP2/aug-cc-PVTZ level of theory.

D1, D2 or from both the forms of the molecule. Interestingly, the *ab initio* calculations show doublet splitting of the band frequency at ~1045 and 1046 cm^{-1}. The former mode at 1045/1044 cm^{-1} belongs to 'A_u'/'B' irreducible representation stemming from dimeric D1/D2 form of the molecule. This mode is IR active but Raman inactive. The other calculated frequency at ~1046 cm^{-1} for D1/D2 forms of the molecule is owed to Raman active totally symmetric 'A_g'/'A' irreducible representations. Doublet splitting of normal modes in dimeric structures is a known observation in quantum chemical calculations and is explicitly reported elsewhere [27]. However the concurrence of both the Raman bands at ~994 and 1053 cm^{-1} may primarily signify the presence of both the dimeric D1 and D2 forms of the HOSA molecule in solid state at room temperature. The presence of either D1 or D2 or both the dimeric forms are further confirmed by the appearance of weak but distinct peaks at ~398, 433, 561 and 616 cm^{-1} in the Raman spectrum.

The high wavenumber window (2500–4000 cm^{-1}) in the Raman spectrum are expected to provide deeper information about the hydrogen bonded N—H vibrations [33–36] of the D1 and/or D2 forms of the HOSA molecule. Many structured bands are noticed in the high frequency region [Fig. 2(a)]. However, the most prominent among them is recorded at ~3473 cm^{-1}. This band ~3473 cm^{-1} [calcd. at 3476/3476.2 cm^{-1} (MP2/aug-cc-pVTZ), 3465.5/3465.7 cm^{-1} (B3LYP/aug-cc-pVTZ) for D1 and 3479/3480 cm^{-1} (MP2/aug-cc-pVTZ), 3504/3505 cm^{-1} (B3LYP/aug-cc-pVTZ) for D2 form of the HOSA molecule] is unambiguously assigned to stretching and bending vibrations of N—H bond linked with hydrogen bond interactions in the D1 and/or D2 forms of the molecule.

Fig. 3(a) shows IR spectrum of HOSA in 400–4000 cm^{-1} wavenumber window recorded at 298 K. The spectra are recorded at room and also at high temperatures ranging from 318 to 418 K [Fig. 3(b–d)]. The corresponding annealed spectrum is shown in Fig. 3(e). The theoretically simulated IR spectra of the D1, D2 and mixed D1, D2 forms of the molecule, as obtained from static *ab initio* calculations, are also shown in Fig. S2. The IR spectrum of HOSA recorded at room temperature is marked by the presence of distinct vibrtional signatures centered at ~430, 588, 994, 1053 and 1230 cm^{-1}. The vibrational analyses [Table 2] reveal that these vibrational signatures emanate either from D1 and/or D2 or from both the dimeric forms of the molecule. This observation may signify the presence of D1 or D2 or from both the forms of the molecule at room temperature and is in line with that inferred from the Raman Spectrum (vide ante). However apart from the presence of both the dimeric forms of the molecule, weak shoulder at ~1533 cm^{-1} and prominent bands at ~1204, 1290, 1400, 1624 cm^{-1} enmark the presence of D1 and D2 forms of the molecule respectively. Interestingly, with rise in temperature, bands at ~1204 and 1400 cm^{-1} gain in intensity with the disappearance of the band at ~1533 cm^{-1}. These results point to explicit presence of D2 form of the molecule at elevated temperatures. The presence of D2 form is also prevalent in the annealed spectrum shown in Fig. 3(e), signifying permanent irreversible deformation of the HOSA molecule with the rise in temperature.

The temperature dependent IR spectra in the high frequency domain (~2200–4000 cm^{-1}) demand considerable attention. This frequency region is marked by the appearance of broad band contour with multiple vibrational signatures ingrained in it. Among these vibrational signatures, the band ~3154 and 3470 cm^{-1} can only be assigned unequivocally. Both these bands are attributed to hydrogen boned N—H stretching and bending vibrations stemming from D1 and/or D2 forms of the molecule. However, appearance of such band contour in the high frequency region is primarily linked to hydrogen bonded N—H vibrations, likely to appear in the dimeric configurations of the molecule than in its monomeric form/forms [37,38]. Significantly enough, the Full Width Half Maximum (FWHM) of the broad band contour (~2200–4000 cm^{-1}) decreases with rise in temperature, signifying some orientational disorder in H – bond bridges and/or in the associated monomers. The significant decrease in the FWHM of the broad band contour ~2200–4000 cm^{-1} wavenumber window with the rise in temperatures may primarily predict the exclusive presence of specific dimeric form of HOSA molecule in solid state at the high temperature domain.

4.3. *Dynamic IR spectra of the dimers form the Fourier transform of DMAF:*

Fig. 4(i, ii) shows room temperature dynamic IR spectra of the D1 and D2 forms of the HOSA molecule as estimated from CPMD and BOMD simulation studies. The temperature dependent dynamic IR spectra of the D1, D2 forms of the molecule as obtained from CPMD and BOMD simulation studies are also shown in Figs. 5 and 6 respectively.

Table 2
Experimentally observed and theoretically simulated vibrational frequencies of the D1 and D2 forms of HOSA molecule as obtained from *ab initio* MP2/aug-cc-pVTZ and also from anharmonic DFT calculations at B3LYP/aug-cc-pVTZ level of theories along with their tentative assignments.

Raman	IR at Room temp.	D1 (C_i)			D2 (C_2)		
		Calcd freq.		Tentative Assignment (PED%) [Symmetry Element]	Calcd freq.		Tentative Assignment (PED %) [Symmetry Element]
		ab initio	DFT		*ab initio*	DFT	
197 (w/sh)						205	$\delta asm_{SO3}(28)\ \tau_{OSON}(25)\ \beta_{SON}(11)\ \beta_{ONH}$ (5) [A]
263 (vw)						268	$\delta sym_{SO3}(62)\ \beta_{SON}(7)\ \tau_{SONH}(7)$ [B]
307 (vvw)					300		$\beta_{SON}(63)\ \delta_{OSO}(23)$ [A]
340 (vvw)						340	$\delta sym_{SO3}(78)\ \beta_{SON}(8)$ [A]
365		355.3	363	$\beta_{OSO}(36)\ \beta_{SON}(22)\ \beta_{ONH}(10)$ [A_g]	356	364	$\delta sym_{SO3}(78)\ \beta_{SON}(8)$ [A]
(vvw)		355.6		$\beta_{OSO}(41)\ \beta_{SON}(20)\ \beta_{ONH}(13)$ [A_u]		366	$\beta_{SON}(67)\ \tau_{SONH}(21)$ [B]
398 (vw)		393	384	$\delta_{OSO}(38)\ \beta_{SON}(29)\ \tau_{SONH}(9)$ [A_g]	389	382	$\delta sym_{SO3}(84)\ \beta_{SON}(12)$ [A]
	430 (vw)	431		$\beta_{SON}(54)$	425		$\beta_{SON}(67)\ \tau_{SONH}(21)$ [B]
433 (w)				$\delta_{OSO}(22)\ \tau_{SONH}(10)$ [A_u]	426		$\beta_{SON}(69)\ \tau_{SONH}(16)$ [A]
565			577.2	$\delta sym_{SO3}(75)\ \beta_{SON}(21)$ [A_u]		573	$\delta sym_{SO3}(56)\ \beta_{SON}(17)\ \delta_{NH3}(10)$ [A]
(w)			577.4	$\delta sym_{SO3}(66)\ \beta_{SON}(28)$ [A_g]			
	588 (vs)	597		$\delta sym_{SO3}(75)\ \beta_{SON}(21)$ [A_u]	594	586	$\delta asm_{SO3}(77)\ r_{SO3}(14)$ [B]
616 (vw)		624	611	$\delta sym_{SO3}(73)\ \nu_{S\text{-}O[NH2]}$ (14) [A_g]	619	624	$\delta sym_{SO3}(53)\ \nu_{S\text{-}O[NH3]}$ (33) [A]
		630		$\delta sym_{SO3}(70)\ \beta_{SON}(13)$ [A_u]	628		$\delta sym_{SO3}(52)\ \nu_{S\text{-}O[NH3]}$ (32) [B]
686 (vw)	690 (vs) 860 (w)						
	994 (s)	1029		$\nu_{ON}(55)\ \nu sym_{SO3}(35)$ [A_u]	1029	1010	$\nu_{ON}(56)\ \nu sym_{SO3}(37)$ [B]
994 (vs)		1016	991	$\nu_{ON}(54)\ \nu sym_{SO3}(35)\ \delta sym_{NH3}(4)$ [A_g]	1017	1011	$\nu_{ON}(55)\ \nu sym_{SO3}(36)$ [A]
	1053(vs)	1045		$\nu_{ON}(45)\ \nu sym_{SO3}(29)\ \delta sym_{NH3}(5)$ [A_u]	1044		$\nu_{ON}(52)\ \nu sym_{SO3}(34)$ [B]
1053 (vvs)		1046		$\nu_{ON}(53)\ \nu sym_{SO3}(34)\ \delta sym_{NH3}(5)$ [A_g]	1046		$\nu_{ON}(54)\ \nu sym_{SO3}(35)$ [A]
1171 (vvw)			1176	δasm_{NH3} (79) [A_g]			
	1204 (vs)		1188	δasm_{NH3} (86) [A_u]	1200	1220	$\delta asm_{NH3}(52)\ \nu sym_{SO3}$ (33) [B]
	1230 (vs)	1232	1237	δasm_{NH3} (86) [A_u]	1239	1234	$\delta asm_{NH3}(72)\nu asm_{SO3}(12)$ [B]
1240		1248	1238	$\delta asm_{NH3}(64)\ \nu asm_{SO3}(24)$ [A_u]		1236	$\delta asm_{NH3}(69)\ \nu asm_{SO3}(24)$ [A]
(vw)		1249		$\delta asm_{NH3}(65)\ \nu asm_{SO3}(17)$ [A_g]	1242		$\delta asm_{NH3}(59)\ \nu asm_{SO3}(27)$ [A]
	1290 (vvs)	1294		$\delta asm_{NH3}(48)\ \nu asm_{SO3}(42)$ [A_u]			
1308			1307	$\nu asm_{SO3}(54)\ \beta_{ONH}$ (31) [A_g]			
(w)			1309	$\nu asm_{SO3}(65)\ \beta_{ONH}(29)$ [A_u]			
	1533 (sh)	1538	1549	δsym_{NH3} (71) β_{ONH} (25) [A_u]			
					1537		$\delta sym_{NH3}(81)\ \beta_{ONH}$ (9) [B]
1534 (w)		1541	1553	δsym_{NH3} (69) β_{ONH} (26) [A_g]	1529		$\delta sym_{NH3}(79)\ \beta_{ONH}$ (11) [A]
	1624 (s)				1624		r_{NH3} (87) [B]
1631 (vvw)					1627		r_{NH3} (93) [A]
		2744	2723	$\nu_{NH}(62)\ \delta_{HNH}(24)$ [A_u]			
2801 (vw)		2803	2785	$\nu_{NH}(57)\ \delta_{HNH}(27)$ [A_g]		2789	$\nu_{NH}(72)\ \delta_{HNH}(19)$ [B]
2870 (vvw)					2884		$\nu_{NH}(67)\ \delta_{HNH}(22)$ [A]
3110 (w/sh)	3127 (s)						
	3154 (s)	3148	3173	$\delta_{HNH}(71)\ \nu_{NH}(29)\delta_{ONH}(7)$ [A_u]	3161		$\delta_{HNH}(49)\ \nu_{NH}(36)\delta_{ONH}(15)$ [B]

(*continued on next page*)

Table 2 (*continued*)

Raman	IR at Room temp.	D1 (C_i)			D2 (C_2)		
		Calcd freq.		Tentative Assignment (PED%) [Symmetry Element]	Calcd freq.		Tentative Assignment (PED %) [Symmetry Element]
		ab initio	DFT		*ab initio*	DFT	
3264 (vvw)						3295	$\delta_{HNH}(49)\ \nu_{NH}(36)\delta_{ONH}(15)$ [B]
						3299	$\delta_{HNH}(43)\ \nu_{NH}(36)\delta_{ONH}(15)$ [A]
	3470 (vs)	3476.0	3465.57	$\nu_{NH}(63)\ \delta_{HNH}(19)\delta_{ONH}(6)$ [A_u]	3479	3504	$\nu_{NH}(52)\ \delta_{HNH}(25)\delta_{ONH}(17)$ [B]
3473 (vs)		3476.2	3465.78	$\nu_{NH}(63)\ \delta_{HNH}(19)\delta_{ONH}(6)$ [A_g]	3480	3505	$\nu_{NH}(51)\ \delta_{HNH}(25)\delta_{ONH}(17)$ [A]

Key: vss, very very strong; vs, very strong; s, strong; w, weak; vw, very weak; vvw, very very weak; sh, shoulder; τ, torsion; β, bending; δ, deformation; δ_{sym}, symmetric deformation; δ_{asm}, asymmetric deformation; r, rocking; ν, stretching; ν_{sym}, symmetric stretching; ν_{asm}, asymmetric stretching; ω, wagging; only contributions ≥ 5 are reported.

The dynamic IR spectra of mixed D1 and D2 forms of the molecule at room temperature, as estimated from CPMD and BOMD calculations [Fig. 4(i, ii) c] both qualitatively reproduce closely with experimentally recorded spectrum [*cf.* Fig. 3(a)]. The noted discrepancy between the experimental and theoretically estimated dynamic IR spectra may be accounted partly due to the anharmonicity of the vibrations. However, the other probable explanation may be the effect of finite fictitious electronic mass parameters that is considered in the CPMD simulation run [29,37,38]. Moreover, the dynamic IR spectrum of the mixed dimeric D1 and D2 forms exhibits structured bands in the low wave number region (0–1700 cm^{-1}) with a broad band envelop in the higher wavenumber window ranging from 2700 to 3000 cm^{-1}. This broad band envelop is explicitly linked with the hydrogen bond interaction and can only be evinced in the D1, D2 and mixed D1, D2 forms of the molecule [Fig. 4(i, ii)]. This is further corroborated from the calculated dynamic IR spectra of the monomeric N- and Z- forms of the HOSA molecule, shown in Fig. S3. Both the spectra, as shown in Fig. S3 feature structured band in the low wavenumber window with no trace of broad band contours in the high wavenumber region. The dynamic IR spectrum, as calculated from the dipole moment of the auto correction

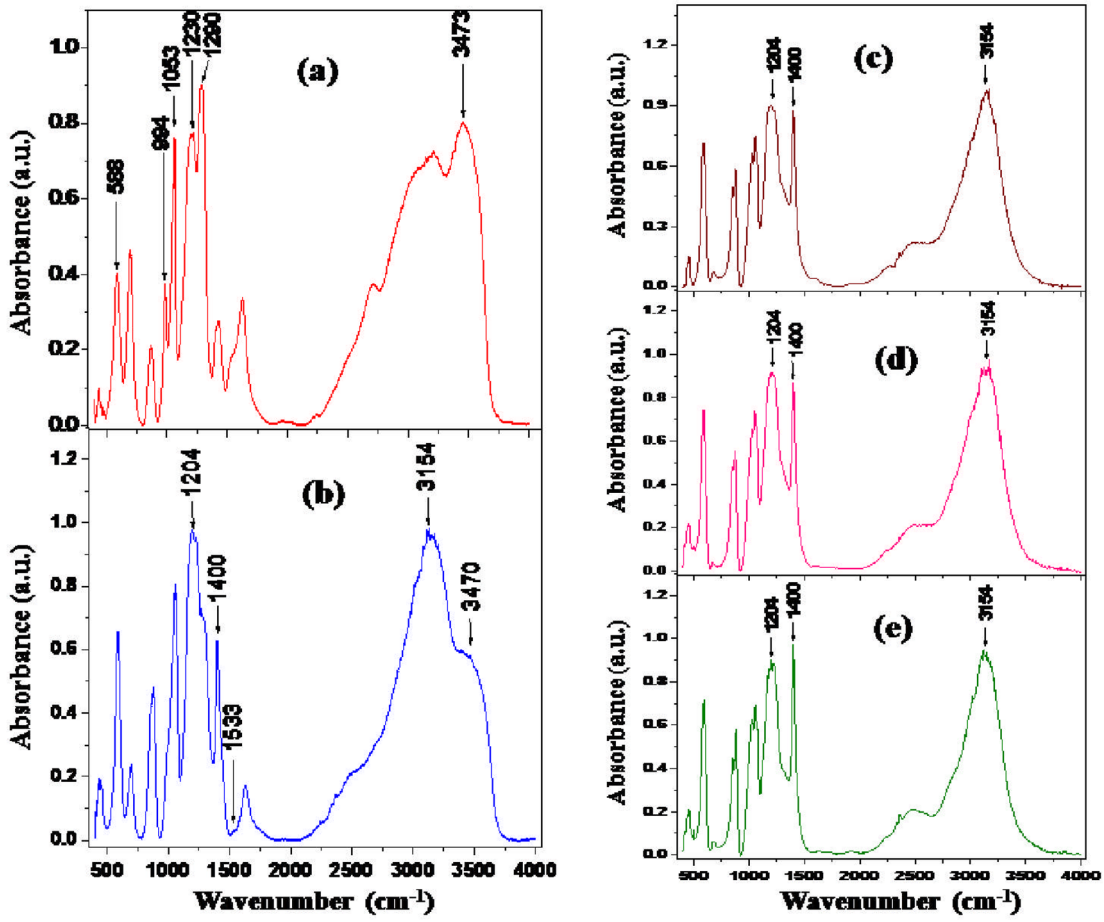

Fig. 3. The FTIR spectra of the HOSA molecule in solid state recorded at (a) 298 K, (b) 318 K, (c) 373 K, (d) 418 K and (e) annealed sample.

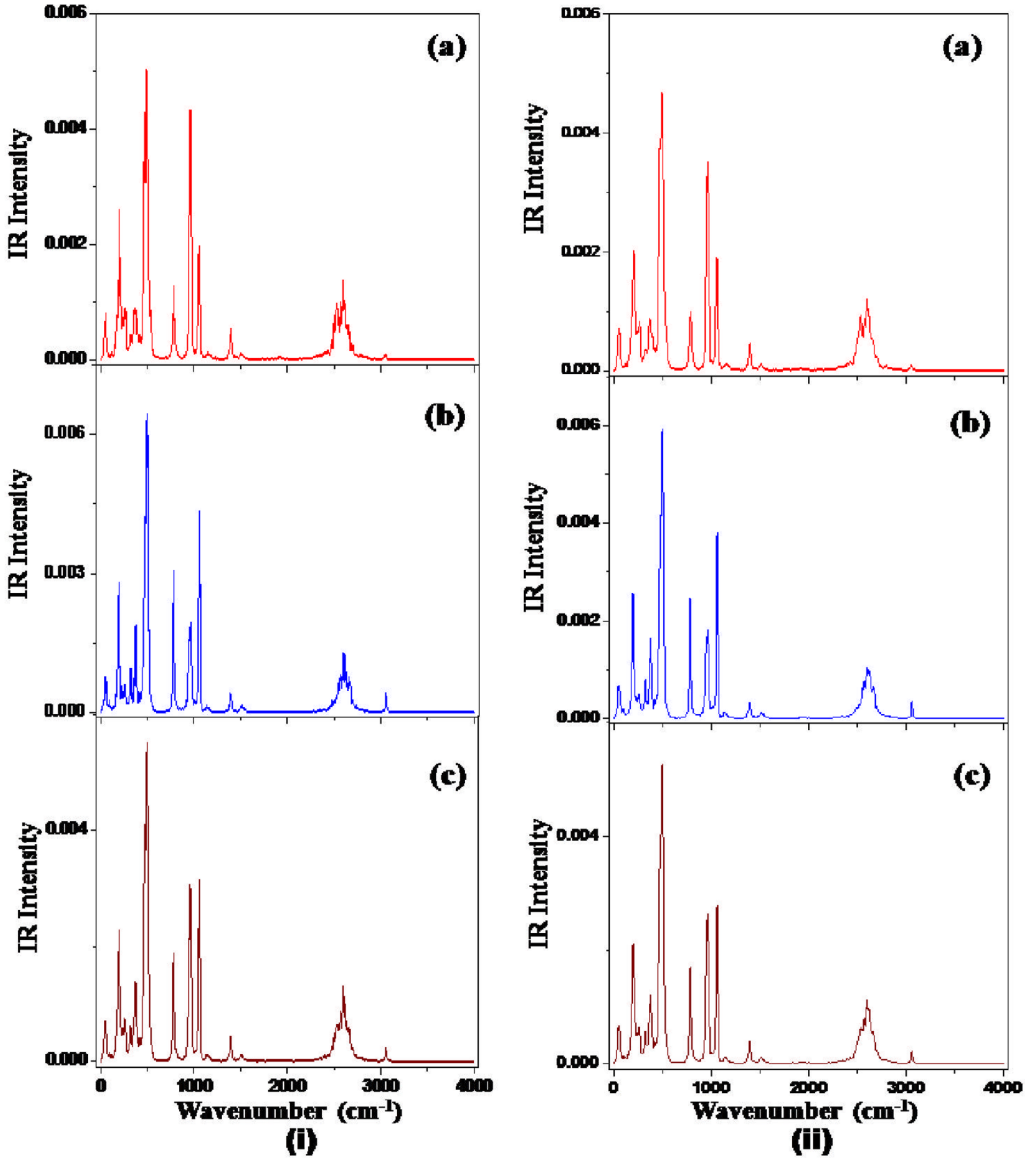

Fig. 4. Simulated gas-phase dynamic IR spectra at 298 K of (a) D1, (b) D2 and (c) mixture of D1, D2 forms of the HOSA molecule as obtained from (i) CPMD and (ii) BOMD calculations.

function indeed has the potential to reproduce vibrational signatures of the molecule involved in hydrogen bond interactions [39,40].

Interesting observation may be drawn from the dynamic IR spectra of the dimeric D1 and D2 forms of HOSA molecule calculated at various temperatures [Figs. 5(a–c)] and 6(a–c)]. The broad band contour in the high wavenumber region is of considerable interest. From Figs. 5(a–c) and 6(a–c), it is seen that with increase in temperature the broad band envelop in the IR spectra of the D1 form of the molecule almost disappear with the appearance of structured bands of reduced line widths. In contrast, calculated IR spectra of the other dimeric D2 form of the molecule [Figs. 5(a–c) and 6(a–c)] still exhibit broad band envelop with rise in temperature.

The evolution of N—H stretching band contours with time for the D2 form of HOSA molecule at various temperatures are estimated from the trajectories so obtained from CPMD and BOMD calculations. They are shown in Fig. S4(a) and (b) respectively. The band contours representing the N-H stretching vibrations of the D2 form of HOSA molecule as shown in Fig. S4(a), (b) also exhibit similar broad band envelop as reflected in Fig. 5(a–c) and 6(a–c) (vide supra). These results may justify both CPMD and BOMD calculations reproduce the experimental observations [Fig. 3(b–d), vide supra] reasonable well and can explain the explicit presence of the dimeric D2 form of HOSA molecule at high temperatures. The disappearance of broad band envelop in the calculated IR spectra of the D1 form of molecule with rise in temperature may auger extirpation of the hydrogen bonded D1 complex at higher temperatures. The temperature dependent dynamic IR spectra thus have the capability to predict the dynamics of hydrogen bonded complex formation or destruction under external perturbation.

5. Conclusion

The Raman and temperature dependent FTIR spectra of HOSA molecule have been recorded. Complete vibrational analyses of the molecule have been estimated for the first time from *ab initio* and anharmonic DFT calculations at MP2/aug-cc-pVTZ and B3LYP/aug-cc-pVTZ level of theories respectively. Both *ab initio* and anharmonic DFT calculations suggest the presence of dimeric D1 and D2 forms of the molecule. The interaction energies (ΔE_{int}) signify the existence of stable dimeric D1, D2 forms of the molecule. The vibrational signatures of the HOSA molecule, as obtained from the Raman and FTIR spectra, also

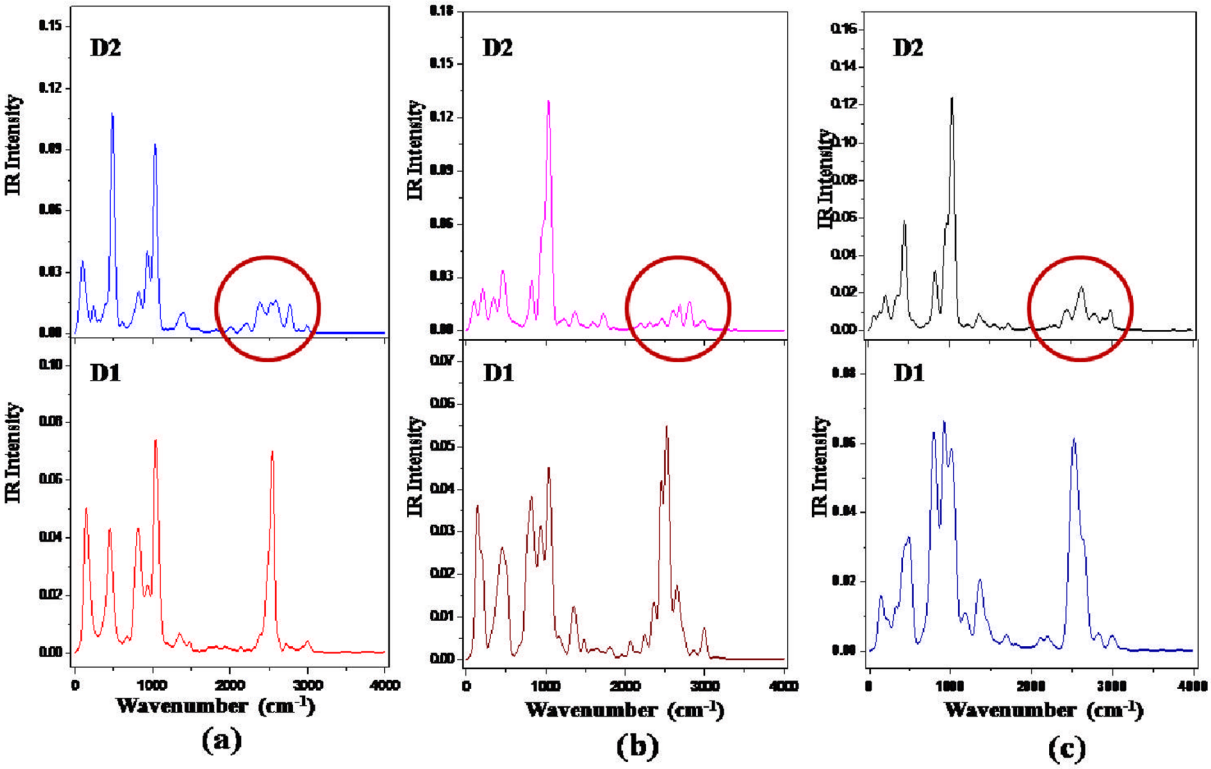

Fig. 5. Simulated gas-phase temperature dependent dynamic IR spectra of D1 and D2 forms of HOSA molecule at (a) 318 K, (b) 373 K and (c) 418 K using CPMD calculations.

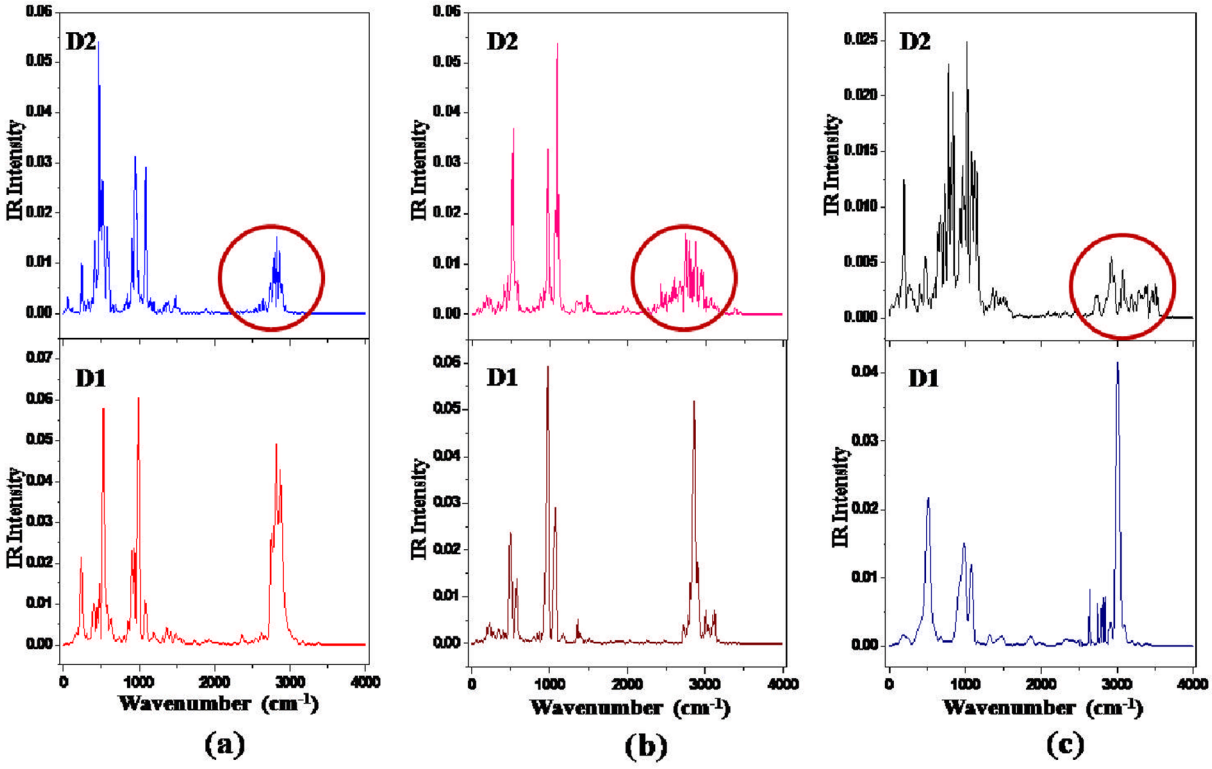

Fig. 6. Simulated gas-phase temperature dependent dynamic IR spectra of D1 and D2 forms of HOSA molecule at (a) 318 K, (b) 373 K and (9c) 418 K using BOMD calculations.

suggest the presence of both the D1 and D2 dimeric forms of the molecule at room temperature. Temperature dependent experimentally observed FTIR in conjunction with dynamic IR spectra, as estimated from CPMD and BOMD calculations, however predict the exclusive presence of D2 dimeric form of HOSA molecule at the high temperature domain.

Declaration of Competing Interest

The authors declare that they have no known competing financial interests or personal relationships that could have appeared to influence the work reported in this paper.

Acknowledgement

Joydeep Chowdhury likes to thank Dr. Takeyuki Tanaka, Integrated Center for Sciences, Ehime University, 3-5-7 Tarumi, Matsuyama, Ehime 790-8566, Japan for providing the high level of computational facility.

Appendix A. Supplementary material

Supplementary data to this article can be found online at https://doi.org/10.1016/j.cplett.2019.136645.

References:

[1] M.H. Abraham, Scales of solute hydrogen-bonding: their construction and application to physicochemical and biochemical processes, Chem. Soc. Rev. 22 (1993) 73–83.
[2] N. Ahmad, H.A. Younus, A.H. Chughtai, F. Verpoort, Metal–organic molecular cages: applications of biochemical implications, Chem. Soc. Rev. 44 (2015) 9–25.
[3] J. Černý, P. Hobza, Non-covalent interactions in biomacromolecules, Phys. Chem. Chem. Phys. 9 (2007) 5291–5303.
[4] P. Hobza, J. Sÿponer, Structure, energetics, and dynamics of the nucleic acid base pairs: nonempirical ab initio calculations, Chem. Rev. 99 (1999) 3247–3276.
[5] J. Sÿponer, P. Hobza, Bifurcated hydrogen bonds in DNA crystal structures. An ab initio quantum chemical study, J. Am. Chem. Soc. 116 (1994) 709–714.
[6] T. Friščić, Supramolecular concepts and new techniques in mechanochemistry: cocrystals, cages, rotaxanes, open metal–organic frameworks, Chem. Soc. Rev. 41 (2012) 3493–3510.
[7] K.C. Leung, K. Lau, Self-assembly and thermodynamic synthesis of rotaxane dendrimers and related structures, Polym. Chem. 1 (2010) 988–1000.
[8] M. Castro, D.R. Salahub, Density-functional calculations for small iron clusters: Fen, Fen+, and Fen- for n < = 5, Phys. Rev. B 49 (1994) 11842–11852.
[9] Y. Li, T.J. Raeker, A.E. Depristo, Step-facilitated dissociation of small metal clusters: a molecular-dynamics study, Phys. Rev. B 50 (1994) 14742–14745.
[10] S.D. Schrøder, J.H. Wallberg, J.A. Kroll, Z. Maroun, V. Vaida, H.G. Kjaergaard, Intramolecular hydrogen bonding in methyl lactate, J. Phys. Chem. A 119 (2015) 9692–9702.
[11] E.J. Ocola, J. Laane, Spectroscopic and theoretical study of the intramolecular π-type hydrogen bonding and conformations of 2-cyclohexen-1-ol, J. Phys. Chem. A 120 (2016) 74–80.
[12] A.S. Özen, F. De Proft, V. Aviyente, P. Geerlings, Interpretation of hydrogen bonding in the weak and strong regions using conceptual DFT descriptors, J. Phys. Chem. A 110 (2006) 5860–5868.
[13] B.A. Omidvar, S.F. Tayyari, M. Vakili, A. Nekoei, Vibrational spectra, normal coordinate analysis, and hydrogen bond investigation of pyridinium perchlorate, Spectrochim. Acta Part A 191 (2018) 558–565.
[14] S. Yalagi, J. Tonannavar, J. Yenagi, Experimental and DFT dimer modeling studies of the H-bond induced-vibration modes of l-β-Homoserine, Spectrochim. Acta Part A 181 (2017) 109–115.
[15] R.E. Asfin, S.M. Melikova, A.V. Domanskaya, P. Rodziewicz, K.S. Rutkowski, Degeneracy lifting effect in the FTIR spectrum of fluoroform trapped in a nitrogen matrix. An experimental and Car−Parrinello molecular dynamics study, J. Phys. Chem. A 120 (2016) 3497–3503.
[16] M.Z. Brela, M.J. Wójcik, M. Boczar, Ł.J. Witek, T. Yonehara, T. Nakajima, Y. Ozaki, Proton dynamics in crystalline tropolone studied by Born-Oppenheimer molecular simulations, Chem. Phy. Lett. 707 (2018) 54–60.
[17] R. Car, M. Parrinello, Unified approach for molecular dynamics and density-functional theory, Phys. Rev. Lett. 55 (1985) 2471–2474.
[18] R.G. Wallace, Hydroxylamine-O –sulfonic acid — a versatile synthetic reagent, Aldrichim. Acta 13 (1980) 3–11.
[19] B. Dutta, T. Tanaka, A. Banerjee, J. Chowdhury, Conformational preferences of ethyl propionate molecule: Raman, temperature dependent FTIR spectroscopic study aided by ab initio quantum chemical and Car-Parrinello molecular dynamics simulation studies, J. Phy. Chem. A 117 (2013) 4838–4850.
[20] B. Dutta, T. Tanaka, J. Chowdhury, Influence of temperature on the rotameric forms of the propyl acetate molecule: Raman and FTIR spectroscopic studies aided by ab initio and Car-Parrinello molecular dynamics simulations, J. Phys. Chem. A 119 (2015) 8062–8075.
[21] M.J. Frisch, G.W. Trucks, H.B. Schlegel, G.E. Scuseria, M.A. Robb, J.R. Cheeseman, G. Scalmani, V. Barone, B. Mennucci, G.A. Petersson, H. Nakatsuji, M. Caricato, X. Li, H.P. Hratchian, A.F. Izmaylov, J. Bloino, G. Zheng, J.L. Sonnenberg, M. Hada, M. Ehara, K. Toyota, R. Fukuda, J. Hasegawa, M. Ishida, T. Nakajima, Y. Honda, O. Kitao, H. Nakai, T. Vreven, J.A. Montgomery Jr., J.E. Peralta, F. Ogliaro, M. Bearpark, J.J. Heyd, E. Brothers, K.N. Kudin, V.N. Staroverov, R. Kobayashi, J. Normand, K. Raghavachari, A. Rendell, J.C. Burant, S.S. Iyengar, J. Tomasi, M. Cossi, N. Rega, J.M. Millam, M. Klene, J.E. Knox, J.B. Cross, V. Bakken, C. Adamo, J. Jaramillo, R. Gomperts, R.E. Stratmann, O. Yazyev, A.J. Austin, R. Cammi, C. Pomelli, J.W. Ochterski, R.L. Martin, K. Morokuma, V.G. Zakrzewski, G.A. Voth, P. Salvador, J.J. Dannenberg, S. Dapprich, A.D. Daniels, O. Farkas, J.B. Foresman, J.V. Ortiz, J. Ciosłowski, D.J. Fox, Gaussian 09W, Revision D.1, Gaussian Inc., Wallingford, CT 06492, USA, 2009.
[22] C. Møller, M.S. Plesset, Note on an approximation treatment for many-electron systems, Phys. Rev. 46 (1934) 618–622.
[23] J.M.L. Martin, V.C. Alsenoy, GAR2PED, University of Aacwerp, 1995.
[24] CPMD, Copyright IBM Corp 1990−2008, Copyright MPI fur Festkorperforschung Stuttgart 1997−2001. http://www.cpmd.org/ (accessed May 18, 2013).
[25] S.A. Nose, A unified formulation of the constant temperature molecular dynamics methods, J. Chem. Phys. 81 (1984) 511–519.
[26] G. Hoover, Canonical dynamics: equilibrium phase-space distributions, Phys. Rev. A 31 (1985) 1695–1697.
[27] J.P. Perdew, S. Burke, M. Ernzerhof, Generalized gradient approximation made simple, Phys. Rev. Lett. 77 (1996) 3865–3868.
[28] N. Troullier, J.L. Martins, Efficient pseudopotentials for plane-wave calculations, Phys. Rev. B 43 (1991) 1993–2006.
[29] B. Dutta, B. Bhattacherjee, J. Chowdhury, Physics behind the Barrier to internal rotation of an acetyl chloride molecule: a combined approach from density functional theory, Car-Parrinello molecular dynamics, and time-resolved wavelet transform theory, ACS Omega 3 (2018) 6794–6803.
[30] N. Bork, V. Loukonen, H.G. Kjaergaard, H. Vehkamaki, Resolving the anomalous infrared spectrum of the MeCN–HCl molecular cluster using ab Initio molecular dynamics, Phys. Chem. Chem. Phys. 16 (2014) 24685–24690.
[31] M. Brehm, B. Kirchner, TRAVIS - a free analyzer and visualizer for Monte Carlo and molecular dynamics trajectories, J. Chem. Inf. Model. 51 (2011) 2007–2023.
[32] N.C. Baenziger, R.F. Belt, C.V. Goebel, Crystal structure of hydroxylamine-O-sulfonic acid, Inorg. Chem. 6 (1967) 511–514.
[33] A. Nataraj, V. Balachandran, T. Karthick, M. Karabacak, A. Atac, FT-Raman, FT-IR, UV spectra and DFT andab initio calculations on monomeric and dimeric structures of 3,5-pyridinedicarboxylic acid, J. Mol. Struc. 1027 (2012) 1–14.
[34] M. Karabacak, E. Kosea, M. Kurtb, FT-Raman, FT-IR spectra and DFT calculations on monomeric and dimeric structures of 5-fluoro- and 5-chloro-salicylic acid, J. Raman Spectrosc. 41 (2010) 1085–1097.
[35] J. Sienkiewicz-Gromiuk, DFT approach to (benzylthio)acetic acid: conformational search, molecular (monomer and dimer) structure, vibrational spectroscopy and some electronic properties, Spectrochim. Acta Part A 189 (2018) 116–128.
[36] D. Bakarić, J. Alerić, T. Parlić-Risović, J. Spanget-Larsen, Hydrogen bonding between ethynyl aromates and triethylamine: IR spectroscopic and computational study, Spectrochim. Acta Part A 209 (2019) 288–294.
[37] M. Karabacak, M. Cinar, FT-IR, FT-Raman, UV spectra and DFT calculations on monomeric and dimeric structure of 2-amino-5-bromobenzoic acid, Spectrochim. Acta Part A 86 (2012) 590–599.
[38] M.A. Palafox, G. Tardajos, A. Guerrero-Martinez, V.K. Rastogi, D. Mishra, S.P. Ojha, W. Kiefer, FT-IR, FT-Raman spectra, density functional computations of the vibrational spectra and molecular geometry of biomolecule 5-aminouracil, Chem. Phys. 340 (2007) 17–31.
[39] M.Z. Brela, M.J. Wojcik, M. Boczar, Ł. Witek, M. Yasuda, Y. Ozaki, Car−Parrinello molecular dynamics simulations of infrared spectra of crystalline vitamin C with analysis of double minimum proton potentials for medium-strong hydrogen bonds, J. Phys. Chem. B 119 (2015) 7922–7930.
[40] M. Brela, J. Stare, G. Pirc, M. Sollner-Dolenc, M. Boczar, M.J. Wójcik, J. Mavri, Car–Parrinello simulation of the vibrational spectrum of a medium strong hydrogen bond by two-dimensional quantization of the nuclear motion: application to 2-hydroxy-5-nitrobenzamide, J. Phys. Chem. B 116 (2012) 4510–4518.